

## 2.2 Control of Elementary Excitations by Acoustic Fields

The research activities on surface acoustic waves (SAWs) are aimed at applications of acoustic fields for the control of elementary excitations such as photons, electrons, spins, and excitons in semiconductor nanostructures. The studies during the year 2007 focused primarily on two topics: the efficient modulation of waveguide structures using SAWs and the development of concepts for the confinement and manipulation of excitons.

Applications of SAWs in integrated optics require new approaches for the acoustic modulation of waveguide structures. Last year, we have proposed and demonstrated a modulation device consisting of a Mach-Zehnder interferometer (MZI), where both interferometer arms are simultaneously modulated by a single SAW beam. This approach allows for the realization of very compact acousto-optic MZIs (a-MZIs), which operate either as modulators or frequency doublers. As a continuation of this work, we have perfected the fabrication process to produce devices with single mode waveguides. Furthermore, we have proposed an extension of the a-MZI concept for structures with several interferometer arms [M. Beck *et al.*, *Appl. Phys. Lett.* **91**, 061118 (2007)]. This novel device concept denoted as acousto-optic multiple interference devices (AOMID), which has been filed as a patent application, allows for the realization of waveguide-based on/off switches, harmonic generator, as well pulse shapers. AOMIDs have been demonstrated to switch light on and off in waveguide structures.

SAW-based acousto-optic devices rely on the modulation of the refractive index by the strain field. They do not require special symmetry properties of the underlying material (such as for electro-optic devices) and can, therefore, be realized in different material systems. We are presently working in collaboration (within the European network ePIXnet) with the Technical University of Denmark and the Technical University of Eindhoven to fabricate a-MZIs and AOMIDs using the silicon-on-insulator and InP technologies, respectively, which are currently the most commonly used technologies for integrated optoelectronic devices operating in the 1550 nm wavelength range. In these devices, the SAWs are generated by interdigital transducers placed on a piezoelectric ZnO island using a process developed at the PDI.

The studies of transport and manipulation of spins using the piezoelectric field of SAWs continued during this year with investigations of spin transport in (100) and (110) quantum wells as well as in (311) quantum wires. For (110) quantum wells, an important result was the demonstration that spins oriented along the growth direction can be transported over distances exceeding 60  $\mu\text{m}$  for temperatures up to at least 77 K. This upper temperature is limited by the efficiency of the used optical technique to probe spin transport. In addition, we have shown that the spin dynamics is very anisotropic and depends strongly on the propagation direction of

the spins on the (110) plane [O. D. D. Couto, Jr. *et al.*, Phys. Rev. Lett. **98**, 036603 (2007)]. These experimental findings initiated investigations, which are aiming at the observation of the transport of optically generated spins up to room temperature. The efficiency of the interconversion process between electron-hole pairs and photons may be increased by embedding the (110) GaAs quantum wells in (Al,Ga)As microcavities.

Previous studies of acoustic transport have used the moving type-II band modulation induced by the piezoelectric field of a SAW to trap and transport electrons and holes. Although effective for the transport of electrons and holes, the piezoelectric field efficiently dissociates excitons and can, therefore, not be used for manipulating them. During this year, we have introduced a new approach for exciton manipulation and transport using the type-I band gap modulation created by the SAW strain field [J. Rudolph *et al.*, Phys. Rev. Lett. **99**, 047602 (2007)]. The experiments have been carried out using SAWs propagating along a  $\langle 100 \rangle$  direction of the (001) surface, which do not carry a longitudinal piezoelectric field. The experiments have been performed using indirect excitons in a double-quantum-well structure. Here, an electric field applied along the growth direction controls the overlap between the wave functions of the electron and the hole forming the exciton and, therefore, the exciton energy and lifetime. Exciton lifetimes on the order of a  $\mu\text{s}$  can be achieved while maintaining the correlation between the electrons and holes. We have shown that these long-living indirect excitons can be transported by the SAW strain field over distances exceeding  $250\ \mu\text{m}$ . This novel approach provides a convenient way for creating microscopic exciton traps for the control of the exciton density, which is an important requirement for the study of exciton-related bosonic effects such as condensation and superfluidity.

After demonstrating SAW-induced transport of magnetic flux-quanta (vortices), we have studied the origin of the concomittant AC-DC conversion effect. This effect, which is often misattributed to directed vortex motion, has been shown to originate in nonlinear interference of the components of the SAW-driving signal. The counterintuitive effect of sign-reversal of the DC signal by exchanging the leads of the RF signal has been elucidated.

### 2.2.1 Acousto-optic multiple interference devices

The modulation of the refractive index induced by the strain field of an acoustic wave offers a powerful tool for light control in waveguides (WG) for integrated optics. Recently, we have demonstrated very efficient and compact light modulators based on the modulation of the arms of a Mach-Zehnder interferometer (MZI) by a surface acoustic wave (SAW) [M. M. de Lima *et al.*, Appl. Phys. Lett. **89**, 121104 (2006)]. Here, we present an extension of this concept to structures with several interferometer arms modulated by a single SAW beam. These acousto-optic multiple interference devices (AOMIDs) provide building blocks for integrated optics for functionalities such as switching, harmonic generation, and pulse shaping. The feasibility of this concept is demonstrated by the realization of an AOMID-based WG device with controllable transmission, which can also be used as an on/off switch for arbitrary time periods.

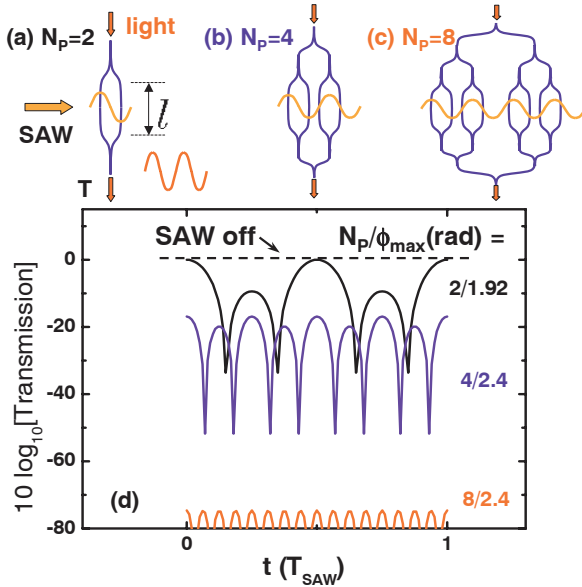


Fig. 14. (a), (b), and (c) Schematic diagrams of AOMIDs with 2, 4, and 8 arms, respectively. (d) Calculated transmission ( $T$ ) as a function of time for AOMIDs with different number of parallel arms ( $N_P$ ) and modulation phases  $\phi_{\text{max}}$ .

AOMID with  $N_P$  arms is given by:

$$T^{(N_P)}(t) = \left| \frac{1}{N_P} \sum_{p=0}^{N_P-1} e^{i\{\phi_{\text{max}} \sin[2\pi(f_{\text{SAW}}t+p)]\}} \right|^2 \stackrel{N_P \rightarrow \infty}{=} J_0^2(\phi_{\text{max}}). \quad (3)$$

where  $f_{\text{SAW}}$  is the acoustic frequency. In the limit  $N_P \rightarrow \infty$ , the transmission becomes time independent and is given by the square of the Bessel function  $J_0(\phi_{\text{max}})$ , which vanishes for  $\phi_{\text{max}} \approx 2.40$  rad. Figure 14(d) compares the time-dependent transmission calculated from Eq. (3) for AOMIDs with different values of  $N_P$ . Note that the transmission for  $N_P \geq 4$  becomes strongly suppressed for  $\phi_{\text{max}} \approx 2.40$ , thus illustrating the operation as a switch with arbitrary on/off times.

Schematic diagrams of AOMIDs with different numbers of arms  $N_P$  arranged in parallel are illustrated in Figs. 14(a)–14(c). The structure with  $N_P = 2$  corresponds to a simple MZI. For simplicity, we will assume that all single-mode WG arms are identical and narrower than the SAW wavelength  $\lambda_{\text{SAW}}$ . The WGs are aligned perpendicular to the SAW propagation direction and displaced laterally to experience SAW phases differing by multiples of  $2\pi/N_P$ . The maximum phase shift  $\phi_{\text{max}}$  of the light propagating through the WGs is related to the WG length  $\ell$  and to the SAW-induced refractive index modulation  $\delta n$  by  $\phi_{\text{max}} = 2\pi\delta n\ell/\lambda_L$ , where  $\lambda_L$  is the light wavelength. Under these assumptions, the transmission  $T^{(N_P)}(t)$  of an

In order to demonstrate the operation of an AOMID as a WG light switch, we have fabricated devices with different numbers of arms on an (Al,Ga)As layer structure. The surface WGs were structured on a 300-nm-thick GaAs core layer deposited by molecular-beam epitaxy on a 1500-nm-thick  $\text{Al}_{0.2}\text{Ga}_{0.8}\text{As}$  cladding layer. The WGs of the AOMID are modulated by a SAW with  $\lambda_{\text{SAW}} = 5.6 \mu\text{m}$  generated by an interdigital transducer (IDT) deposited on the sample surface. Figure 15(a) displays a schematic diagram of a six-fold AOMID, which uses multimode interference couplers (MMI) to connect the interferometer arms to the input and output WGs. Time-resolved transmission traces for this device recorded for different acoustic powers (in terms of the nominal rf-voltage  $V_{\text{rf}}$  applied to the IDT) are displayed in Fig. 15(b). In agreement with Fig. 14(d), the average transmission reduces with  $V_{\text{rf}}$  and reaches a minimum of about 5% ( $\approx 13$  dB) for  $V_{\text{rf}} = 4$  V, demonstrating the feasibility of the arbitrary switching operation.

The residual transmission of the device in Fig. 15 in the off (i.e., light-blocking) state is significantly higher than the one expected from calculations for devices with  $N_P \geq 4$  [see Fig. 14(d)]. The high residual transmission has been traced back to imperfections during fabrication, which introduces differences in the light coupling efficiency and the optical path length ( $\delta\ell$ ) of the different arms. In fact, the measured residual transmission in the off state can be accounted for by assuming an effective difference in lengths of the interferometer arms of only 40 nm over a total arm length of  $120 \mu\text{m}$  [M. Beck *et al.*, Appl. Phys. Lett. **91**, 061118 (2007)], which is comparable to the tolerances of the fabrication process using optical lithography with a nominal resolution of approx.  $0.5 \mu\text{m}$ . The asymmetries also account for the transmission modulation at the first (observed for  $1.2 < V_{\text{rf}} < 2.9$  V) and second harmonic of  $f_{\text{SAW}}$  (for  $2.9 \text{ V} < V_{\text{rf}}$ ). In fact, the transmission of a perfectly symmetric device with an even number  $N_P$  of arms is invariant under a SAW phase change of  $2\pi/N_P$  [cf. Fig. 15(a)] and should, therefore, only contain harmonics of  $N_P f_{\text{SAW}}$ . Considerably higher switching contrasts are then expected from improvements in the fabrication tolerances.

In conclusion, we have demonstrated an extended concept for acousto-optic interference devices, which are waveguide based and compatible with integrated optics. We have shown that efficient light modulators, harmonic generators, and attenuators can be realized by modulating MZIs composed of several arms using a single SAW beam.

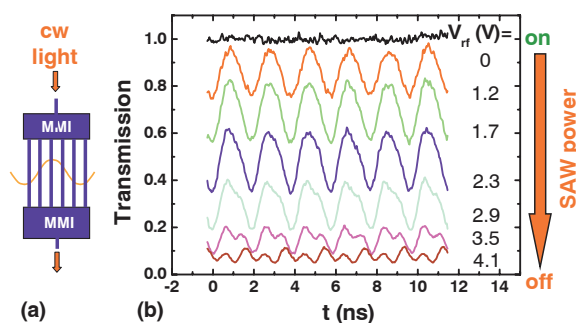


Fig. 15. (a) A 6-fold AOMID using multimode interference couplers (MMIs) to couple the light to the multiple interferometer arms and (b) time-dependent optical transmission measured for different rf-voltages  $V_{\text{rf}}$  applied to the acoustic transducer.

(M. Beck, M.M. de Lima, Jr.\*, E. Wiebicke, W. Seidel, R. Hey, P. V. Santos

\*University of Valencia, Valencia, Spain)

### 2.2.2 Long-range exciton transport by surface acoustic waves in GaAs quantum wells

The strong interaction with light makes excitons very interesting excitations for coherent manipulation using photons. In addition, excitons are expected to follow the Bose-Einstein statistics in the low-density regime and thus to exhibit collective bosonic effects like superfluidity and Bose-Einstein condensation. The observation of these effects requires a tool to transport excitons in a controlled way as well as to efficiently trap them in order to control their density.

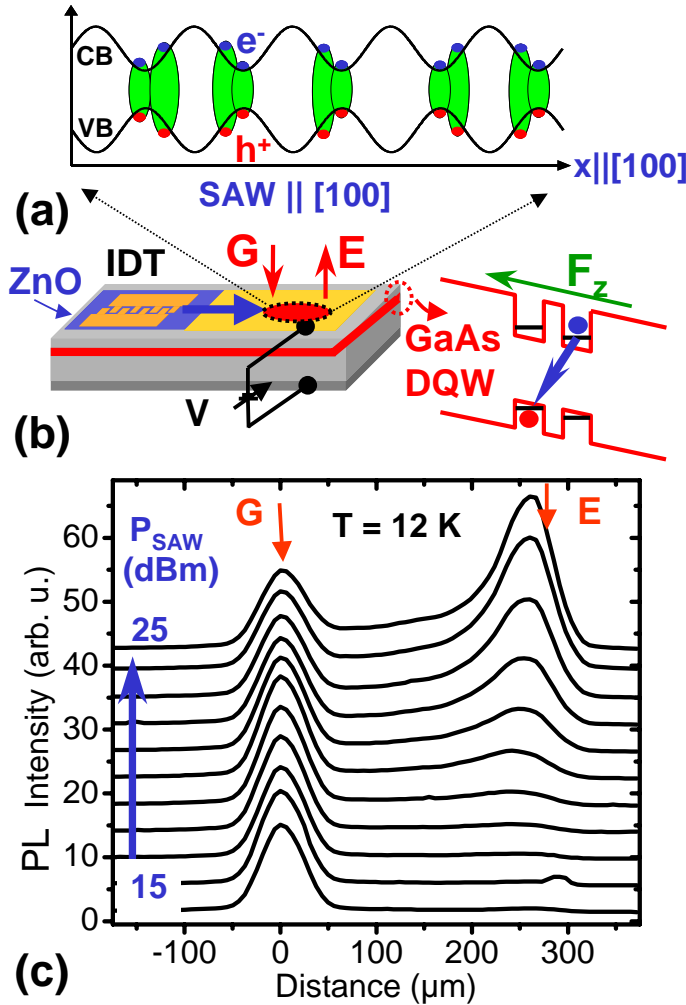


Fig. 16. (a) A SAW propagating along the  $x=[100]$  direction of the (001) surface GaAs produces a moving type-I modulation of the CB and VB band edges of a GaAs DQW structure, which transports excitons. (b) Sample and band diagram along the growth ( $z$ ) direction, showing the formation of indirect excitons by the application of an electric field  $F_z$ . (c) Experimental evidence for the transport of indirect excitons using spatially resolved photoluminescence (PL). For strong acoustic powers  $P_{\text{SAW}}$ , photogenerated excitons are transported from the photo-generation point G to the edges of the metal gate E.

using a Rayleigh SAW along the  $x = [100]$  direction, which does not carry a longitudinal piezoelectric field. These waves can be generated by using interdigital transducers (IDTs) deposited on a piezoelectric ZnO island, as illustrated in Fig. 16(b).

Here, we introduce a novel approach for exciton confinement and transport using the strain field of a surface acoustic wave (SAW). Via the deformation potential interaction, the SAW strain induces a type-I modulation of the conduction band (CB) and valence band (VB) edges, as illustrated in Fig. 16(a). Excitons are trapped at the positions of the minimum band gap and transported by the moving field with the acoustic velocity  $v_{\text{SAW}}$ . In contrast to the conventional ambipolar transport of electrons and holes, which relies on the type-II modulation by the SAW piezoelectric field, the electrons and holes constituting the excitons are trapped in the same spatial positions along the SAW propagation direction  $x$ .

For a piezoelectric Rayleigh SAW propagating along the  $[110]$  direction of the (001) GaAs substrates, the modulation of the potential by piezoelectric effects exceeds the strain-related modulation by almost two orders of magnitude. In order to prevent exciton dissociation by the piezoelectric field, the transport experiments were carried out

Two further conditions have to be satisfied to achieve long-range exciton transport using acoustic fields. First, in order to obtain the long lifetimes (i.e., much longer than the acoustic period  $T_{\text{SAW}}$ ) required for acoustic transport, we have used long-living indirect excitons in a double quantum well (DQW) structure separated by a thin (i.e., smaller than the exciton radius) barrier [cf. Fig. 16(b)]. Here, an electric field  $F_z$  along the growth direction ( $z$ ) forces the Coulomb-coupled electrons and holes into different quantum wells (QWs). The spatial separation along the  $z$ -direction allows for lifetime control up to the ms range while keeping the Coulomb correlation between the particles. The second condition for transport is that the exciton drift velocity  $v_{\text{exc}} = \mu_{\text{ex}} |\partial \Delta E_g(x) / \partial x|^{\text{max}}$  must exceed the acoustic velocity  $v_{\text{SAW}}$ , where  $\mu_{\text{ex}}$  and  $\Delta E_g(x)$  denote the exciton mobility and the amplitude of the band gap modulation, respectively. Due to interface scattering,  $\mu_{\text{ex}}$  increases with the sixth power of the QW thickness [Z. Vörös *et al.*, Phys. Rev. Lett. **97**, 016803 (2006)]. Using the experimentally determined values for the band gap modulation amplitudes  $\Delta E_g$  of approx. 2 meV measured in the structures of Fig. 16(b), one can show that the last requirement can be satisfied for QWs with thickness above 14 nm.

The acoustically induced transport of excitons was investigated by generating excitons using a laser beam focused at spot G [cf. Fig. 16(b)] on the SAW path and detecting the photoluminescence (PL) along the  $x$  direction with a spatial resolution of a few  $\mu\text{m}$ . Photoluminescence profiles recorded for a fixed gate-voltage  $V = -8$  V [cf. Fig. 16(b)] and increasing nominal rf-powers  $P_{\text{SAW}}$  applied to the IDT are illustrated in Fig. 16(c). For  $P_{\text{SAW}} < 20$  dBm, PL emission occurs only at the generation point G, thus indicating that transport does not take place. For higher SAW powers ( $P_{\text{SAW}} \geq 20$  dBm), emission emerges at the edge E of the top-gate located about  $300 \mu\text{m}$  away from G. We attribute the PL at E to the recombination of excitons transported from the generation spot G by the mobile SAW modulation. The quantum-confined Stark effect induced by the gate voltage lowers the exciton energy underneath the top-gate as compared to the surrounding unbiased regions. This potential barrier at the edge E blocks the transport and forces the excitons to recombine, leading to the strong emission. The emission from E increases with  $P_{\text{SAW}}$ , indicating an improved transport efficiency as the amplitude of the strain-induced modulation increases. Furthermore, excitonic transport has been only observed for sufficiently large gate voltages (and, therefore, large vertical fields  $F_z$ ), which further demonstrates the excitonic character of the transport and reinforces the importance of using long-living indirect excitons.

In summary, we have demonstrated the acoustic transport of excitons over several hundreds of  $\mu\text{m}$  in DQW structures. Additional experiments have shown that the excitons remain confined within a region with dimensions on the order of a  $\mu\text{m}$  during transport, thus establishing SAWs as a convenient tool for exciton manipulation.

(J. Rudolph, R. Hey, P.V. Santos)

### 2.2.3 AC-DC conversion effect in high- $T_c$ superconductors

There is great effort to demonstrate induced directed motion of magnetic vortices in superconductors for fundamental reasons and because of far reaching technological consequences related to the field of fluxtronics. The activities center around so-called vortex-ratchet experiments, where directed vortex motion is achieved by asymmetric patterning of pinning structures. A more flexible way of vortex control, the surface-acoustic-wave driven vortex transport, was demonstrated by us recently. This approach requires no defect-structuring, no intricately modulated drive signal and in principle allows for fine-tuning of the direction and speed of vortex motion. In many ratchet experiments AC-DC conversion is taken as proof for directed vortex motion. We show, however, that AC-DC conversion is a natural and common effect in systems with nonlinear current-voltage characteristics — it does not require a ratchet, and it is not necessarily a sign of directed vortex motion.

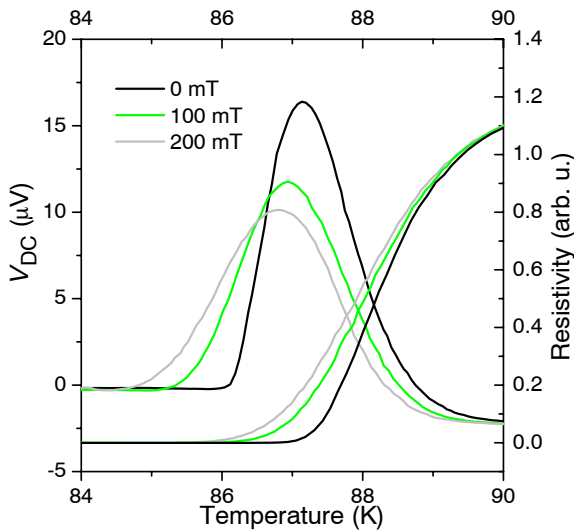


Fig. 17. Temperature dependence of  $V_{DC}(T)$  and  $R(T)$  for different magnetic background fields. The field is oriented perpendicular to the film.  $V_{DC}(T)$  follows the broadening and temperature shift of the resistive transition.

We investigated 100 nm films of granular  $\text{YBa}_2\text{Cu}_3\text{O}_7$  grown on y-cut  $\text{LiNbO}_3$  substrates. The samples are contacted for 4-point measurements. The application of an AC current leads to a DC voltage drop at the resistive transition. This signal is independent of whether  $I_{AC}$  is applied directly to the sample or eddy currents are impressed through induction by an RF electromagnetic field. Figure 17 shows that the peak of  $V_{DC}$  broadens with increasing applied magnetic field and shifts to lower temperatures in accordance with the resistive transition of the superconductor. The AC-DC conversion was observed almost identically in different samples over a wide range of frequencies. As a striking

feature, a sign-reversal in the DC-signal by interchanging the leads of the AC driving-current was reproducibly observed. The result of reversing the polarity of the AC connection is shown in Fig. 18. The change of the polarity of the AC connectors reverses the signal almost completely. In order to rule out that this rather counterintuitive behavior is related to the asymmetry of the AC source or the leads, we eliminated asymmetries in the experimental setup that could define the direction of  $V_{DC}$ . The samples were processed in a symmetric layout, and the only significant electrical asymmetry possibly present was in the RF leads as coaxial transmission lines are generally unbalanced. In this experiment, the source was balanced by an RF transformer (BALUN). The impedance was matched to a symmetric 100  $\Omega$  transmission line built out of two parallel 50  $\Omega$  coaxial transmission lines. Both AC terminals had the same potential

to ground. Still, the same DC voltage drop at  $T_c$  was observed as well as the sign reversal of  $V_{DC}$  on a reversal of AC polarity.

The subject of AC-DC conversion in superconductors has been widely discussed in the early years of high- $T_c$  superconductivity and a wide range of theoretical explanations of varying complexity have been employed to explain this effect. A simple approach was chosen by S. Ikegawa *et al.* [J. Appl. Phys. **64**, 5061 (1988)], who viewed the superconductor as an element with a nonlinear current-voltage relation. In this case, the  $V(I)$  characteristic expanded to 3rd order is simply given by

$$V(I) = V(0) + \frac{dV}{dI} \Big|_0 I + \frac{1}{2!} \frac{d^2V}{dI^2} \Big|_0 I^2 + \frac{1}{3!} \frac{d^3V}{dI^3} \Big|_0 I^3. \quad (4)$$

According to S. Ikegawa *et al.*, the DC potential along the current path results from the superposition of the first and second harmonic of the rf drive-signal. Inserting their respective amplitudes  $I_{rf1}$  and  $I_{rf2}$  into Eq. (4) and considering a phase shift of  $\phi$  between both components yields

$$V_{DC} = \frac{dV^2}{dI^2} \Big|_0 \left( \frac{I_{rf1}^2 + I_{rf2}^2}{4} \right) + \frac{dV^3}{dI^3} \Big|_0 \left( -\frac{I_{rf1}^2 I_{rf2}}{8} \sin \phi \right) \quad (5)$$

for the DC component of the induced voltage. The first term in Eq. (5) can be described as a conventional rectification process, while the second term expresses an effect of *nonlinear interference* between fundamental and harmonic frequencies. A reversed polarity of  $I_{AC}$  can be expressed as a sign reversal of  $I_{rf1}$  or as a phase-shift of  $180^\circ$  between both components. While  $I_{rf1}$  appears in Eq. (5) only to the power of two, the sign of  $I_{rf2}$  determines the sign of the nonlinear interference term.

In Fig. 18(b), the two components of the induced DC voltage have been extracted from the experimental data. One can discern a small, rectified component, which does not change sign with a reversed AC polarity, and the component generated by nonlinear interference that flips sign on reversing  $I_{AC}$ . The rectified voltage follows the superconducting transition and might therefore be linked to thermal contact potentials. We have shown that in order to prove induced, directed vortex motion by AC-DC conversion the influence of nonlinear interference has to be ruled out.

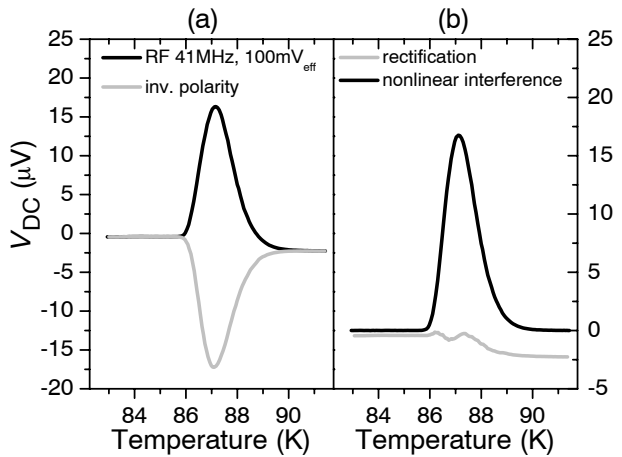


Fig. 18. (a) Induced DC voltage as a function of temperature for two polarities of the applied driving current. (b) The components of the induced DC voltage due to rectification (grey line) and nonlinear interference (black line) as a function of temperature.